IJST, Transactions of Electrical Engineering, Vol. 38, No. E1, pp 33-57
Printed in The Islamic Republic of Iran, 2014

TWO-DIMENSIONAL ANALYTICAL MAGNETIC FIELD CALCULATIONS FOR DOUBLY-SALIENT MACHINES*

A. RAHIDEH**, H. MOGHBELLI[2] AND T. KORAKIANITIS[3]

[1]School of Electrical and Electronic Engineering, Shiraz University of Technology, Shiraz, I. R. of Iran
Email: rahide@sutech.ac.ir
[2]Arak University of Technology, Arak, I. R. of Iran
[3]Parks College of Engineering, Aviation and Technology, Saint Louis University, Saint Louis, MO 63013, USA

Abstract– This paper investigates a 2-dimensional (2-D) analytical magnetic field prediction for doubly-salient machines. Using the subdomain technique, the effects of saliency on both the rotor and stator structures as well as their interactions are considered. The approach can be used for magnetic field calculation in machines with any combination of rotor- and stator-pole number. Three different stator winding structures are considered: non-overlapping winding with all teeth wound, non-overlapping winding with alternate teeth wound and 2-layer overlapping winding. To enable the analytical solution of the governing partial differential equations, the stator and rotor iron is assumed to be infinitely permeable and therefore the saturation effects are neglected. The proposed approach is used in two case studies: (1) to calculate the armature reaction magnetic field distribution of a three-phase slotted brushless machine with surface inset magnets and (2) to compute the magnetic field distribution of a four-phase switched reluctance motor. Note that the proposed approach cannot be employed in the case of machines with considerable saturation effects. The analytical results are compared with those obtained from finite element analyses to validate the analytical calculations.

Keywords– Subdomain, brushless machines, switched reluctance machine, surface inset magnet

1. INTRODUCTION

Doubly-salient machines have saliency on both the stationary and movable parts. Some well-known examples of doubly-salient machines are switched reluctance motors (SRMs); slotted brushless machines with surface inset permanent magnets (PMs) on movable part; and doubly-salient machines with magnets on stator. Similar to other electric machines, doubly-salient machines can be classified, in terms of their motion, as rotary and linear in which rotary motion machines are further categorized, according to their flux direction, as radial-, axial- and transverse-flux machines. In this investigation, the focus is only on radial-flux, rotary motion doubly-salient machines without any magnet on stator.

Electromagnetic devices can be modelled and analyzed either analytically or numerically. Although numerical approaches, such as the finite element method (FEM), are widely employed to analyze the performance of designed machines, their applications during the design procedure are limited mostly to the final validation stage. This is because numerical techniques are time-consuming, hardly provide facilities to systematically change the topology of the under study device and give no physical insight to the problem. Therefore, analytical solutions, if possible, are preferred in the inherently iterative design process of an electromagnetic device. Despite the mentioned advantages of analytical techniques, they, unlike numerical techniques, are normally incapable of accommodating the saturation effects of nonlinear media and have less flexibility to solve problems with complex geometries.

*Received by the editors June 22, 2013; Accepted May 7, 2014.
**Corresponding author

Slotted brushless machines with surface inset magnets have a doubly-salient structure where the stator slots house the windings and the magnets are normally placed between two adjacent rotor saliencies. Since the relative permeability of PMs is close to unity, the machines are electro-magnetically deemed as double-salient despite the cylindrical appearance of the rotor. Brushless PM machines having surface inset magnets have several advantages compared to those having surface mounted magnets due to the presence of the iron inter-poles. Some of them include: better rotor mechanical robustness, especially at higher speeds; lower PM eddy current losses; the ability to develop reluctance torque; higher quadrant- per direct-axis inductance ratio; and a wider flux weakening region.

There is an increasing number of studies reported in the literature dealing with two-dimensional (2-D) analytical magnetic field calculations of brushless PM machines [1]-[50]; however, just a small number of them concern the surface inset magnet structure [42]-[49]. The magnetic field of brushless PM machines originates from two different sources: magnets and armature winding current. One of the applications of this study is the armature reaction field calculation of slotted brushless machines equipped with surface inset magnets. Zhu et al. [42] have presented an analytical open-circuit magnetic field calculation for slotless brushless machines with surface inset magnets having radial magnetization. Rahideh and Korakianitis [43]-[44] have extended the work proposed in [42] to other magnetization patterns such as parallel and Halbach. Note that [42]-[44] have reported the open-circuit magnetic field computation for slotless stator machines. The open-circuit magnetic field calculation of slotted brushless machines with radially magnetized surface inset magnets has been reported in [45] where the depth of stator slots is assumed to be infinite. Although it has taken into account the effects of double-salient structures, only the open circuit magnetic field has been investigated. Boughrara et al. [46] have presented both open-circuit and armature reaction field calculations of brushless PM machines having surface inset or surface mounted magnets using the Schwarz-Christoffel transformation; however, the approach is deemed more numerical than analytical. Analytical armature reaction field calculations for slotless brushless machines equipped with inset magnets have been reported in [47]. The analytical magnetic field computations of slotted brushless machines having surface inset magnets can be found in [48] and [49].

The switched reluctance motor is one of the simplest doubly-salient motors from a manufacturing viewpoint but one of the most challenging machines from the modelling perspective. The stator slots of radial-flux, rotary motion SRMs normally accommodate non-overlapping (concentric) windings while rotor has neither winding nor PM. Therefore unlike brushless PM machines, the only source of the magnetic field in SRMs is the stator winding current. Some of the advantages of SRMs include simple manufacturability, cost effectiveness, mechanical robustness, relatively high power density, high speed operation capability, four-quadrant operation capability with unidirectional current, flexible and versatile drive features, negligible mutual inductance between phase windings, high short-term overload capability, fault tolerant capabilities and hazard-free operation. Despite these outstanding features, SRMs suffer from a number of drawbacks such as high torque ripples, sensitivity to air-gap length and therefore to rotor eccentricity, producing noise, requirement of a converter even for constant speed applications and necessity of magnetic saturation to maximize power density. In addition, the motor inductance is a function of both rotor position (due to rotor saliency) and the excitation current (due to iron saturation) which increases the complexity of high performance controllers. The theory of switched reluctance motor controllers is not as well-known as it is in the case of other motors such as induction or brushless PM motors. Owing to these unique features, SRMs found their applications in some critical cases – such as aircraft actuators, coolant pump in nuclear power plants, and electric vehicles – where high reliability in hazardous environment is a vital factor. Due to the significance of switched reluctance machines in such crucial applications, their design and analysis require special attention. It should also be noted that the modelling of switched reluctance machines is more challenging compared to that of induction or brushless

PM machines because, first, the magnetic saturation of rotor/stator back-iron necessitates nonlinear study, especially at aligned rotor positions and second, the coupling between the flux linkage, phase currents and rotor position increases the complexity of SRM modelling.

The developed torque of an electric motor can be calculated using different approaches. The most common methods are: (1) virtual work which is based on the change in co-energy; (2) Maxwell's stress tensor which requires an accurate calculation of the magnetic flux density distribution at an arbitrary surface in the air-gap region; (3) the product of induced back-emf and armature current divided by rotational velocity (and neglecting or, if possible, taking into account the magnetic losses) provided that the back-emf and armature current are either inherently independent or orthogonal (e.g. in separately excited dc motors) or can be transformed into an orthogonal form (e.g. induction motors using the field-oriented control). In the case of SRMs, the first two approaches are viable for torque calculation but the last technique is hardly possible as a simple transformation to provide the required orthogonality is not available.

If the flux-linkage could be expressed as a function of current and rotor angular position, the co-energy and subsequently the developed torque would be calculated. Torrey and Lang [51] have proposed an empirical flux-linkage expression based on experimental data extracted at different rotor positions and under a range of current levels. Miller and McGilp [52] used piecewise first- or second-order functions to analytically model the nonlinear magnetization characteristics of SRMs in which flux linkage is presented against rotor position with current as a parameter (unlike previous attempts [53] in which flux linkage was represented as a function of current with rotor position as a parameter). Xia et al. [54] have extended Miller model [52] by incorporating the flux linkage expression proposed in [51]. Lovatt [55] has studied three modelling techniques for switched reluctance motors: (1) a simple equivalent circuit model based on infinitely permeable iron which therefore neglects the saturation effects; (2) a two-model approach corresponding to below and above the flux saturating point; (3) the torque is empirically assumed to have a linear relationship with current above the saturation point. Lin et al. [56] have developed an analytical dynamic model for switched reluctance motors in which the flux linkage has been expressed by multiple decoupled one-argument functions. None of the abovementioned researches [51]-[56] considered a 2-D analytical model.

As mentioned before, another approach of torque calculation is based on Maxwell's stress tensor integral which requires an accurate calculation of the radial and tangential components of the magnetic flux density distribution at an arbitrary surface in the air-gap region. Lubin et al. [57] have presented a 2-D analytical magnetic field calculation in the air-gap of cylindrical electric machines considering slotting effects. The analytical model is applicable to electric machines having only rotor saliency since the stator is assumed to be cylindrical; therefore the proposed model cannot accurately calculate the magnetic field distribution of doubly-salient machines such as switched reluctance machines or slotted brushless machines with surface inset magnets. The applications of SRMs in electric vehicles have comprehensively been investigated in [58]. Useful information on the optimal design of SRMs can be found in [59]. The effects of non-uniform air-gap on SRM noise problems have been investigated in [60].

In this paper, a 2-D analytical magnetic field calculation is proposed for double-salient machines. The derived analytical expressions can be used to calculate the armature reaction field of slotted brushless machines with surface inset magnets or the magnetic field of switched reluctance machines if the flux density remains below the saturation point. Even in the case of switched reluctance machines under saturation effects, the approach can be employed to analyze the unaligned rotor position which is difficult to be accurately investigated using conventional magnetic equivalent circuit methods.

2. PROBLEM FORMULATION

To analytically calculate the magnetic field distribution of a doubly-salient machine, the following steps are normally performed:

1. Make a set of assumptions to enable the analytical solution.
2. Divide the problem domain into a number of subdomains according to the assumptions, the geometry and the electromagnetic properties of each part of the machine.
3. Derive the governing partial differential equations (PDEs) for each subdomain based on Maxwell's equations and the assumptions made.
4. Define a set of boundary/interface conditions based on the subdomains and their geometries.
5. Represent the winding current density distribution as a function of time and spatial position.
6. Find a general solution for each subdomain to satisfy the governing PDEs and to also have the potential to satisfy the boundary/interface conditions.
7. Impose the boundary/interface conditions to determine the integration constants of the general solutions.
8. Validate the analytical results using the normal finite element method.

a) Assumptions

In this study the following assumptions are made,

- End effects are ignored.
- The magnetic flux density is a 2-D vector with radial and tangential components. Therefore the magnetic vector potential has only *z*-component.
- The magnetic flux density vector and the magnetic vector potential are independent of *z*.
- All materials are isotropic.
- One tooth per pole is assumed.
- The stator and rotor teeth have no tooth-tip.
- The rotor/stator iron is infinitely permeability; therefore the saturation effects are neglected.
- The slots and rotor poles have radial sides.
- Eddy current reaction field is neglected.

b) Subdomains

The active subdomains consist of stator slots, air-gap and rotor slots due to the infinite permeability assumption of the stator and rotor back-iron. In a machine with N_s stator poles and N_r rotor poles, as shown in Fig. 1, with non-overlapping windings the number of subdomains is N_s+N_r+1. Indices *sl*, *a* and *ra* in Fig. 1 denote slots, air-gap and airspace between rotor iron-poles. In the case of 2-layer overlapping windings each slot is radially divided into two sub-regions and instead of index *sl*, indices *slt* and *slb* are used for the top and bottom parts of the slots. Subsequently the number of sub-regions will be $2N_s+N_r+1$.

c) Governing equations

The following Maxwell equations are employed to initiate the derivation of the governing PDE-based equations:

$$\nabla \times \mathbf{H} = \mathbf{J} \tag{1}$$

$$\nabla \cdot \mathbf{B} = 0 \tag{2}$$

where $\mathbf{H}$ is the magnetic field intensity vector, $\mathbf{J}$ is the winding current density vector and $\mathbf{B}$ is the magnetic flux density vector. The magnetic field intensity and magnetic flux density vectors are related by

the following expression in a linear medium.

$$\mathbf{B} = \mu_0 \mu_r \mathbf{H}\,, \tag{3}$$

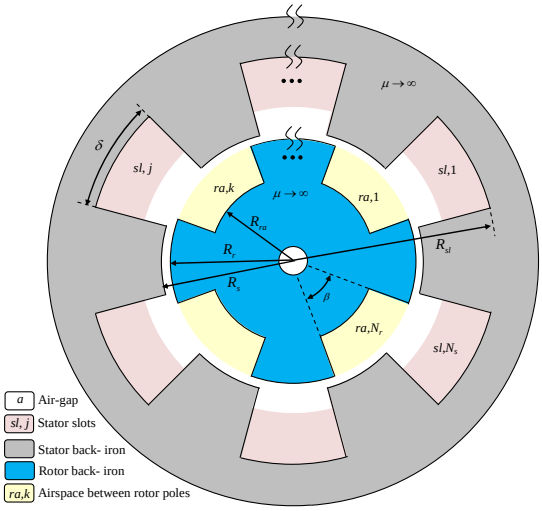

Fig. 1. Illustrative representation of the subdomains in a doubly-salient machine

where μ_0 is the free space permeability and μ_r is the relative permeability of the medium. Substituting (3) in Ampere's law, (1), yields

$$\nabla \times \mathbf{B} = \mu_0 \mu_r \mathbf{J} \tag{4}$$

Based on Gauss's law for magnetism, (2), $\mathbf{B}$ is divergence free and can be written in terms of the vector magnetic potential as

$$\mathbf{B} = \nabla \times \mathbf{A} \tag{5}$$

Substituting (5) in (4) and by choosing Coulomb gauge, $\nabla \cdot \mathbf{A} = 0$, the governing equation can be expressed as

$$\nabla^2 \mathbf{A} = -\mu_0 \mu_r \mathbf{J} \tag{6}$$

In this study, the doubly-salient machine consists of air-gap, airspace between rotor iron-poles and stator slots regions with the following Poisson's and Laplace's equations:

$$\nabla^2 \mathbf{A}^{sl} = -\mu_0 \mathbf{J} \tag{7}$$

$$\nabla^2 \mathbf{A}^{i} = \mathbf{0} \qquad i = \{a, ra\} \tag{8}$$

where superscripts *a*, *ra*, and *sl* denote air-gap, airspace between the rotor iron-poles, and stator slots regions, respectively. In the case of 2-D problems in polar coordinates, it is assumed that $\mathbf{A} = [0, 0, A_z(r,\theta)]$, $\mathbf{J} = [0, 0, J_z(\theta, t)]$ and from (5)

$$\begin{aligned} B_r(r,\theta) &= \frac{1}{r}\frac{\partial A_z}{\partial \theta} \\ B_\theta(r,\theta) &= -\frac{\partial A_z}{\partial r}. \end{aligned} \tag{9}$$

Therefore, (7) and (8) can be rewritten as

$$\frac{1}{r}\frac{\partial}{\partial r}\left(r\frac{\partial A_z^{sl}}{\partial r}\right) + \frac{1}{r^2}\frac{\partial^2 A_z^{sl}}{\partial \theta^2} = -\mu_0 J_z \tag{10}$$

$$\frac{1}{r}\frac{\partial}{\partial r}\left(r\frac{\partial A_z^i}{\partial r}\right)+\frac{1}{r^2}\frac{\partial^2 A_z^i}{\partial \theta^2}=0 \qquad i=\{a,ra\}. \tag{11}$$

d) Boundary conditions

The perpendicular component of the magnetic flux density vector is continuous at the interface between two adjacent media. If the interface is source-free, then the parallel component of the magnetic field intensity vector on one side of the boundary is equal to that of the other side. Also, the parallel component of the magnetic field intensity vector is zero at the interface of those media adjacent to infinitely permeable domains. Therefore the following boundary conditions are expressed:

$$H_\theta^{ra,k}(r,\theta)|_{R=R_{ra}}=0 \tag{12}$$

$$H_r^{ra,k}(r,\theta)|_{\theta=\alpha+2\pi(k-0.5)/N_r\pm\beta/2}=0 \tag{13}$$

$$B_r^a(r,\theta)|_{r=R_r}=B_r^{ra,k}(r,\theta)|_{r=R_r} \qquad \left|\theta-\alpha-\tfrac{2(k-0.5)\pi}{N_r}\right|\le\tfrac{\beta}{2} \tag{14}$$

$$H_\theta^a(r,\theta)|_{r=R_r}=\begin{cases}\sum_{k=1}^{N_r}H_\theta^{ra,k}(r,\theta)|_{r=R_r} & \left|\theta-\alpha-\tfrac{2(k-0.5)\pi}{N_r}\right|\le\tfrac{\beta}{2}\\ 0 & \text{elsewhere}\end{cases} \tag{15}$$

$$B_r^a(r,\theta)|_{r=R_s}=B_r^{sl,j}(r,\theta)|_{r=R_s} \qquad \theta_j-\tfrac{\delta}{2}\le\theta\le\theta_j+\tfrac{\delta}{2} \tag{16}$$

$$H_\theta^a(r,\theta)|_{r=R_s}=\begin{cases}\sum_{j=1}^{N_s}H_\theta^{sl,j}(r,\theta)|_{r=R_s} & \theta_j-\tfrac{\delta}{2}\le\theta\le\theta_j+\tfrac{\delta}{2}\\ 0 & \text{elsewhere}\end{cases} \tag{17}$$

$$H_r^{sl,j}(r,\theta)|_{\theta=\theta_j\pm\delta/2}=0 \tag{18}$$

$$H_\theta^{sl,j}(r,\theta)|_{R=R_{sl}}=0 \qquad \theta_j-\tfrac{\delta}{2}\le\theta\le\theta_j+\tfrac{\delta}{2} \tag{19}$$

for $k=1,2,\ldots,N_r$ and $j=1,2,\ldots,N_s$ where N_r and N_s are respectively the number of rotor and stator poles, β is the span angle of rotor airspace opening, δ is the span angle of each stator slot, as shown in Fig. 1, α is the rotor angular position and $\theta_j=2\pi(j-0.5)/N_s$ is the angular position of the centre of slot j.

e) Current density distribution

Current waveforms of a q-phase machine can be expressed by their Fourier series expansion as

$$i_\kappa(t)=I_0+\sum_w I_w\sin\left[w(p\omega t-\gamma_\kappa)+\theta_w\right] \qquad \kappa=1,2,\ldots,q \tag{20}$$

where I_w and θ_w are the amplitude and phase shift of the w-th harmonic of the phase current, I_0 is the average current of each phase, $\gamma_\kappa=2\pi(\kappa-1)/q$ is the temporal phase shift angle of κ-th phase with respect to the first phase, ω is the rotational velocity and p is an integer number which depends on the number of rotor poles (N_r) and the motor type. For instance, in brushless PM machines $p=N_r/2$ whereas in the case of switched reluctance machines $p=N_r$. Therefore, the fundamental frequency of the current in each phase is expressed as follows

$$f_1=\frac{\omega}{2\pi}p \tag{21}$$

which in a switched reluctance motor is twice as high as a brushless PM motor with identical number of rotor poles.

In order to relate the currents of all phases to the current density in each slot, the connecting matrix is used. It is a $q\times N_s$ matrix with each entry being 1, 0 or -1 where 0 at the κ,j-th entry means there is no coil

of phase κ in slot *j*. 1 or -1, respectively, means the positive or negative side of one of the coils of phase κ is located in slot *j*. In the case of non-overlapping windings with alternate teeth wound, the current density vector of all slots can be found as $\mathbf{J}(t)=k_f\mathbf{i}(t)\mathbf{C}/A_c$ where k_f is the winding filling factor, A_c is the wire cross sectional area, $\mathbf{C}$ is the connecting matrix, $\mathbf{J}(t)=\begin{bmatrix}J^1(t) & J^2(t) & \cdots & J^{N_s}(t)\end{bmatrix}$ and $\mathbf{i}(t)=\begin{bmatrix}i_1(t) & i_2(t) & \cdots & i_q(t)\end{bmatrix}$. As is obvious from the expression, the current density of each slot is independent of θ since the winding is single-layer.

In the case of non-overlapping windings with all teeth wound, the current density of each slot can be found as

$$J^j(\theta,t)=J_0^j(t)+\sum_{v=1}^{\infty}J_v^j(t)\cos\left(\tfrac{\pi v}{\delta}\left(\theta-\theta_j+\delta/2\right)\right)$$
$$\theta_j-\delta/2\le\theta\le\theta_j+\delta/2. \tag{22}$$

For 2-layer non-overlapping winding, the coefficients of the current density Fourier series expansion are expressed as

$$J_0^j(t)=\frac{J_\ell^j(t)+J_r^j(t)}{2} \tag{23}$$

$$J_v^j(t)=\frac{J_\ell^j(t)-J_r^j(t)}{\pi v/2}\sin(\pi v/2) \tag{24}$$

where $J_\ell^j(t)$ and $J_r^j(t)$ are respectively the current density of the coils located in the left and right sides of slot *j* (observing from the motor centre) at time *t*, defined respectively as $\mathbf{J}_r(t)=k_f\mathbf{i}(t)\mathbf{C}_r/A_c$ and $\mathbf{J}_\ell(t)=k_f\mathbf{i}(t)\mathbf{C}_\ell/A_c$ where $\mathbf{J}_r(t)=\begin{bmatrix}J_r^1(t) & J_r^2(t) & \cdots & J_r^{N_s}(t)\end{bmatrix}$, $\mathbf{J}_\ell(t)=\begin{bmatrix}J_\ell^1(t) & J_\ell^2(t) & \cdots & J_\ell^{N_s}(t)\end{bmatrix}$ and $\mathbf{C}_r$ and $\mathbf{C}_\ell$ are connecting matrices of the right and left sides of slots, respectively. More details on winding currents are given in Appendix A.

f) General solutions

The general solution of the Poisson equation in the airspace between the rotor iron-poles is

$$A_z^{ra,k}(r,\theta)=b_0^{ra,k}\ln r+\sum_{u=1}^{\infty}\left[a_u^{ra,k}\left(\frac{r}{R_r}\right)^{\frac{\pi u}{\beta}}+b_u^{ra,k}\left(\frac{R_{ra}}{r}\right)^{\frac{\pi u}{\beta}}\right]$$
$$\times\cos\left(\tfrac{\pi u}{\beta}\left(\theta-\alpha-\tfrac{2(k-0.5)\pi}{N_r}+\tfrac{\beta}{2}\right)\right). \tag{25}$$

Applying the boundary condition stated in (12) reduces the general solution in the magnet regions to

$$A_z^{ra,k}(r,\theta)=\sum_{u=1}^{\infty}a_u^{ra,k}\left[\left(\frac{r}{R_r}\right)^{\frac{\pi u}{\beta}}+\left(\frac{R_{ra}}{R_r}\right)^{\frac{\pi u}{\beta}}\left(\frac{R_{ra}}{r}\right)^{\frac{\pi u}{\beta}}\right]$$
$$\times\cos\left(\tfrac{\pi u}{\beta}\left(\theta-\alpha-\tfrac{2(k-0.5)\pi}{N_r}+\tfrac{\beta}{2}\right)\right). \tag{26}$$

The general solution of the Laplace equation in the air-gap can be represented as

$$A_z^a(r,\theta)=\sum_{n=1}^{\infty}\left[a_n^a\left(\frac{r}{R_s}\right)^n+b_n^a\left(\frac{R_r}{r}\right)^n\right]\cos(n\theta)$$
$$+\left[c_n^a\left(\frac{r}{R_s}\right)^n+d_n^a\left(\frac{R_r}{r}\right)^n\right]\sin(n\theta). \tag{27}$$

In the case of non-overlapping windings, the general solution of the Poisson equation in the stator slots is expressed as

$$A_z^{sl,j}(r,\theta) = b_0^{sl,j}\ln r + A_p^{sl,j}(r,\theta) + \sum_{v=1}^{\infty}\left[a_v^{sl,j}\left(\frac{r}{R_{sl}}\right)^{\frac{\pi v}{\delta}} + b_v^{sl,j}\left(\frac{R_s}{r}\right)^{\frac{\pi v}{\delta}}\right] \times \cos\left(\tfrac{\pi v}{\delta}\left(\theta-\theta_j+\tfrac{\delta}{2}\right)\right) \tag{28}$$

where the particular solution is

$$A_p^{sl,j}(r,\theta) = -\frac{\mu_0}{4}J_0^j r^2 + \sum_{v=1}^{\infty}\frac{\mu_0 J_v^j r^2}{\left(\frac{\pi v}{\delta}\right)^2-4}\cos\left(\tfrac{\pi v}{\delta}\left(\theta-\theta_j+\tfrac{\delta}{2}\right)\right). \tag{29}$$

Applying the boundary condition stated in (19) yields

$$A_z^{sl,j}(r,\theta) = \frac{\mu_0 J_0^j}{4}\left(2R_{sl}^2\ln r - r^2\right) + \sum_{v=1}^{\infty}\left\{b_v^{sl,j}\left[\left(\frac{R_s}{R_{sl}}\right)^{\frac{\pi v}{\delta}}\left(\frac{r}{R_{sl}}\right)^{\frac{\pi v}{\delta}} + \left(\frac{R_s}{r}\right)^{\frac{\pi v}{\delta}}\right] + \frac{\mu_0 J_v^j}{\left(\frac{\pi v}{\delta}\right)^2-4}\left[r^2 - \frac{2R_{sl}^2}{\frac{\pi v}{\delta}}\left(\frac{r}{R_{sl}}\right)^{\frac{\pi v}{\delta}}\right]\right\} \times \cos\left(\tfrac{\pi v}{\delta}\left(\theta-\theta_j+\tfrac{\delta}{2}\right)\right). \tag{30}$$

In the case of machines with 2-layer overlapping windings, each slot is radially divided into two equal-area regions: the bottom and top parts of the slot which are denoted by superscripts *slb* and *slt*, respectively. The general solutions in the bottom and top parts of each slot are respectively expressed as follows after applying (19) and also the continuity conditions between two media to derive the integration constants of the top part of the slots in terms of those of the bottom part.

$$A_z^{slt,j}(r,\theta) = \frac{\mu_0}{2}\left[J_{b0}^j\left(R_{sl}^2-R_{slm}^2\right)\ln r + J_{t0}^j\left(R_{slm}^2\ln r - \tfrac{1}{2}r^2\right)\right] + \sum_{v=1}^{V}b_v^{sl,j}\left[\left(\frac{R_{slm}}{R_{sl}}\right)^{\frac{\pi v}{\delta}}\left(\frac{r}{R_{sl}}\right)^{\frac{\pi v}{\delta}} + \left(\frac{R_{slm}}{r}\right)^{\frac{\pi v}{\delta}}\right] \times \cos\left(\tfrac{\pi v}{\delta}\left(\theta-\theta_j+\tfrac{\delta}{2}\right)\right) \tag{31}$$

$$A_z^{slb,j}(r,\theta) = \frac{\mu_0 J_{b0}^j}{2}\left(R_{sl}^2\ln r - \tfrac{1}{2}r^2\right) + \sum_{v=1}^{V}b_v^{sl,j}\left[\left(\frac{R_{slm}}{R_{sl}}\right)^{\frac{\pi v}{\delta}}\left(\frac{r}{R_{sl}}\right)^{\frac{\pi v}{\delta}} + \left(\frac{R_{slm}}{r}\right)^{\frac{\pi v}{\delta}}\right] \times \cos\left(\tfrac{\pi v}{\delta}\left(\theta-\theta_j+\tfrac{\delta}{2}\right)\right). \tag{32}$$

where $R_{slm} = \sqrt{\left(R_{sl}^2+R_s^2\right)/2}$ is the radius which radially divides each slot into two equal-area regions and J_{b0}^j and J_{t0}^j are the current density in the bottom and top parts of the slots, respectively.

The number of integration constants to be determined is $4N+N_sV+N_rU$ consisting of a_n^a, b_n^a, c_n^a and d_n^a, (for $n=1,\ldots,N$), $b_v^{sl,1},\ldots,b_v^{sl,N_s}$ (for $v=1,\ldots,V$) and $a_u^{ra,1},\ldots,a_u^{ra,N_r}$ (for $u=1,\ldots,U$) where *N*, *V* and *U* are the number of harmonics in the air-gap, stator slot and airspace between rotor iron-poles regions, respectively.

g) Integration constants calculation

Boundary conditions (14)-(17) equate two waveforms with different fundamental frequency for a predefined interval. Therefore the correlation technique should be employed [50].

- Multiplying both sides of (14) by $\frac{2}{\beta}\sin\left(\frac{\pi u}{\beta}\left(\theta-\alpha-\frac{2(k-0.5)\pi}{N_r}+\frac{\beta}{2}\right)\right)$, integrating over $\left[\alpha+\frac{2(k-0.5)\pi}{N_r}-\frac{\beta}{2},\ \alpha+\frac{2(k-0.5)\pi}{N_r}+\frac{\beta}{2}\right]$, i.e.

$$\begin{aligned}&\frac{2}{\beta}\int_{\alpha+2(k-0.5)\pi/N_r-\beta/2}^{\alpha+2(k-0.5)\pi/N_r+\beta/2} B_r^a\mid_{r=R_r}\ \sin\left(\frac{\pi u}{\beta}\left(\theta-\alpha-\frac{2(k-0.5)\pi}{N_r}+\frac{\beta}{2}\right)\right)d\theta\\&=\frac{2}{\beta}\int_{\alpha+2(k-0.5)\pi/N_r-\beta/2}^{\alpha+2(k-0.5)\pi/N_r+\beta/2} B_r^{ra,k}\mid_{r=R_r}\ \sin\left(\frac{\pi u}{\beta}\left(\theta-\alpha-\frac{2(k-0.5)\pi}{N_r}+\frac{\beta}{2}\right)\right)d\theta,\end{aligned}\tag{33}$$

and using orthogonality of trigonometric functions, the following N_rU equations for $u=1,2,\ldots,U$ and $k=1,2,\ldots,N_r$ are obtained

$$\begin{aligned}&\frac{\pi u}{\beta}\left[1+\left(\frac{R_{ra}}{R_r}\right)^{\frac{2u\pi}{\beta}}\right]a_u^{ra,k}-\sum_{n=1}^{N} n\left\{\left[a_n^a\left(\frac{R_r}{R_s}\right)^n+b_n^a\right]\sigma_s(n,u,k)\right.\\&\left.-\left[c_n^a\left(\frac{R_r}{R_s}\right)^n+d_n^a\right]\sigma_c(n,u,k)\right\}=0\end{aligned}\tag{34}$$

where

$$\begin{aligned}&\sigma_s(n,u,k)=\\&\frac{2}{\beta}\int_{\alpha+2(k-0.5)\pi/N_r-\beta/2}^{\alpha+2(k-0.5)\pi/N_r+\beta/2}\sin(n\theta)\sin\left(\frac{\pi u}{\beta}\left(\theta-\alpha-\frac{2(k-0.5)\pi}{N_r}+\frac{\beta}{2}\right)\right)d\theta\end{aligned}\tag{35}$$

$$\begin{aligned}&\sigma_c(n,u,k)=\\&\frac{2}{\beta}\int_{\alpha+2(k-0.5)\pi/N_r-\beta/2}^{\alpha+2(k-0.5)\pi/N_r+\beta/2}\cos(n\theta)\sin\left(\frac{\pi u}{\beta}\left(\theta-\alpha-\frac{2(k-0.5)\pi}{N_r}+\frac{\beta}{2}\right)\right)d\theta.\end{aligned}\tag{36}$$

The integral solutions are given in Appendix B.

- Multiplying both sides of (15) by $\frac{1}{\pi}\sin(n\theta)$, integrating over $[\alpha-\pi,\ \alpha+\pi]$, i.e.

$$\begin{aligned}&\frac{1}{\pi}\int_{\alpha-\pi}^{\alpha+\pi} H_\theta^a\mid_{r=R_r}\ \sin(n\theta)d\theta\\&=\frac{1}{\pi}\sum_{k=1}^{N_r}\int_{\alpha+2(k-0.5)\pi/N_r-\beta/2}^{\alpha+2(k-0.5)\pi/N_r+\beta/2} H_\theta^{ra,k}\mid_{r=R_r}\ \sin(n\theta)d\theta,\end{aligned}\tag{37}$$

and similarly using orthogonality of trigonometric functions, the following N equations for $n=1,2,\ldots,N$ are obtained

$$\sum_{k=1}^{N_r}\sum_{u=1}^{U}\frac{u\pi}{\beta}\left[\left(\frac{R_{ra}}{R_r}\right)^{\frac{2u\pi}{\beta}}-1\right]\rho_s(n,u,k)a_u^{ra,k}+n\left[c_n^a\left(\frac{R_r}{R_s}\right)^n-d_n^a\right]=0\tag{38}$$

where

$$\begin{aligned}&\rho_s(n,u,k)=\\&\frac{1}{\pi}\int_{\alpha+2(k-0.5)\pi/N_r-\beta/2}^{\alpha+2(k-0.5)\pi/N_r+\beta/2}\cos\left(\frac{u\pi}{\beta}\left(\theta-\alpha-\frac{2(k-0.5)\pi}{N_r}+\frac{\beta}{2}\right)\right)\sin(n\theta)\,d\theta\end{aligned}\tag{39}$$

and the integral solution is represented in Appendix B.

- Multiplying both sides of (15) by $\frac{1}{\pi}\cos(n\theta)$ and integrating over $[\alpha-\pi,\alpha+\pi]$, i.e.

$$\begin{aligned}&\frac{1}{\pi}\int_{\alpha-\pi}^{\alpha+\pi} H_\theta^a\mid_{r=R_r}\ \cos(n\theta)d\theta\\&=\frac{1}{\pi}\sum_{k=1}^{N_r}\int_{\alpha+2(k-0.5)\pi/N_r-\beta/2}^{\alpha+2(k-0.5)\pi/N_r+\beta/2} H_\theta^{ra,k}\mid_{r=R_r}\ \cos(n\theta)d\theta,\end{aligned}\tag{40}$$

yields the following N equations for $n=1,2,\ldots,N$:

$$\sum_{k=1}^{N_r}\sum_{u=1}^{U}\frac{u\pi}{\beta}\left[\left(\frac{R_{ra}}{R_r}\right)^{\frac{2u\pi}{\beta}}-1\right]\rho_c(n,u,k)a_u^{ra,k}+n\left[a_n^a\left(\frac{R_r}{R_s}\right)^n-b_n^a\right]=0 \tag{41}$$

where

$$\rho_c(n,u,k)= \frac{1}{\pi}\int_{\alpha+2(k-0.5)\pi/N_r-\beta/2}^{\alpha+2(k-0.5)\pi/N_r+\beta/2}\cos\left(\frac{u\pi}{\beta}\left(\theta-\alpha-\frac{2(k-0.5)\pi}{N_r}+\frac{\beta}{2}\right)\right)\cos(n\theta)\,d\theta. \tag{42}$$

The solution of the integral is represented in Appendix B.

- Multiplying both sides of (17) by $\frac{1}{\pi}\cos(n\theta)$ and integrating over $[-\pi,\pi]$, i.e.

$$\begin{aligned}&\frac{1}{\pi}\int_{-\pi}^{\pi}H_\theta^a(r,\theta)|_{r=R_s}\cos(n\theta)d\theta\\&=\frac{1}{\pi}\sum_{j=1}^{N_s}\int_{\theta_j-\delta/2}^{\theta_j+\delta/2}H_\theta^{sl,j}(r,\theta)|_{r=R_s}\cos(n\theta)d\theta,\end{aligned} \tag{43}$$

results in the following N equations for $n=1,2,\ldots,N$:

$$\begin{aligned}&n\left[a_n^a-b_n^a\left(\frac{R_r}{R_s}\right)^n\right]-\sum_{j=1}^{N_s}\sum_{v=1}^{V}\frac{\pi v}{\delta}\left[\left(\frac{R_s}{R_{sl}}\right)^{\frac{2\pi v}{\delta}}-1\right]\eta_c(n,v,j)b_v^{sl,j}\\&=\sum_{j=1}^{N_s}\frac{\mu_0 J_0^j}{2}\left(R_{sl}^2-R_s^2\right)\eta_c(n,0,j)\\&+\sum_{j=1}^{N_s}\sum_{v=1}^{V}\frac{2\mu_0 J_v^j}{\left(\frac{\pi v}{\delta}\right)^2-4}\left[R_s^2-R_{sl}^2\left(\frac{R_s}{R_{sl}}\right)^{\frac{\pi v}{\delta}}\right]\eta_c(n,v,j)\end{aligned} \tag{44}$$

where

$$\eta_c(n,v,j)=\frac{1}{\pi}\int_{\theta_j-\delta/2}^{\theta_j+\delta/2}\cos(n\theta)\cos\left(\frac{\pi v}{\delta}\left(\theta-\theta_j+\frac{\delta}{2}\right)\right)d\theta. \tag{45}$$

The integral is solved in Appendix B.

- Similarly multiplying both sides of (17) by $\frac{1}{\pi}\sin(n\theta)$ and integrating over $[-\pi,\pi]$, i.e.

$$\begin{aligned}&\frac{1}{\pi}\int_{-\pi}^{\pi}H_\theta^a(r,\theta)|_{r=R_s}\sin(n\theta)d\theta\\&=\frac{1}{\pi}\sum_{j=1}^{N_s}\int_{\theta_j-\delta/2}^{\theta_j+\delta/2}H_\theta^{sl,j}(r,\theta)|_{r=R_s}\sin(n\theta)d\theta,\end{aligned} \tag{46}$$

yields the following N equations for $n=1,2,\ldots,N$:

$$\begin{aligned}&n\left[c_n^a-\left(\frac{R_r}{R_s}\right)^n d_n^a\right]-\sum_{j=1}^{N_s}\sum_{v=1}^{V}\frac{\pi v}{\delta}\left[\left(\frac{R_s}{R_{sl}}\right)^{\frac{2\pi v}{\delta}}-1\right]\eta_s(n,v,j)b_v^{sl,j}\\&=\sum_{j=1}^{N_s}\frac{\mu_0 J_0^j}{2}\left(R_{sl}^2-R_s^2\right)\eta_s(n,0,j)\\&+\sum_{j=1}^{N_s}\sum_{v=1}^{V}\frac{2\mu_0 J_v^j}{\left(\frac{\pi v}{\delta}\right)^2-4}\left[R_s^2-R_{sl}^2\left(\frac{R_s}{R_{sl}}\right)^{\frac{\pi v}{\delta}}\right]\eta_s(n,v,j)\end{aligned} \tag{47}$$

where

$$\eta_s(n,v,j)=\frac{1}{\pi}\int_{\theta_j-\delta/2}^{\theta_j+\delta/2}\sin(n\theta)\cos\left(\frac{\pi v}{\delta}\left(\theta-\theta_j+\frac{\delta}{2}\right)\right)d\theta \tag{48}$$

and its solution is given in Appendix B.

- Multiplying both sides of (16) by $\frac{2}{\delta}\sin\left(\frac{\pi\nu}{\delta}\left(\theta-\theta_j+\frac{\delta}{2}\right)\right)$ and integrating over $\left[\theta_j-\frac{\delta}{2},\theta_j+\frac{\delta}{2}\right]$, i.e.

$$\begin{aligned}&\frac{2}{\delta}\int_{\theta_j-\delta/2}^{\theta_j+\delta/2}B_r^{sl,j}(r,\theta)|_{r=R_s}\sin\left(\frac{\pi\nu}{\delta}\left(\theta-\theta_j+\frac{\delta}{2}\right)\right)d\theta\\&=\frac{2}{\delta}\int_{\theta_j-\delta/2}^{\theta_j+\delta/2}B_r^{a}(r,\theta)|_{r=R_s}\sin\left(\frac{\pi\nu}{\delta}\left(\theta-\theta_j+\frac{\delta}{2}\right)\right)d\theta,\end{aligned}\tag{49}$$

results in the following VN_s equations for $j=1,2,\ldots,N_s$ and $\nu=1,2,\ldots,V$:

$$\begin{aligned}&-\sum_{n=1}^{N}n\left\{\left[a_n^a+b_n^a\left(\frac{R_r}{R_s}\right)^n\right]\varepsilon_s(n,\nu,j)\right.\\&\left.-\left[c_n^a+d_n^a\left(\frac{R_r}{R_s}\right)^n\right]\varepsilon_c(n,\nu,j)\right\}\\&+\frac{\pi\nu}{\delta}\left[\left(\frac{R_s}{R_{sl}}\right)^{\frac{2\pi\nu}{\delta}}+1\right]b_\nu^{sl,j}\\&=-\frac{\mu_0 J_\nu^j}{\left(\frac{\pi\nu}{\delta}\right)^2-4}\left[\frac{\pi\nu}{\delta}R_s^2-2R_{sl}^2\left(\frac{R_s}{R_{sl}}\right)^{\frac{\pi\nu}{\delta}}\right]\end{aligned}\tag{50}$$

where

$$\varepsilon_s(n,\nu,j)=\frac{2}{\delta}\int_{\theta_j-\delta/2}^{\theta_j+\delta/2}\sin(n\theta)\sin\left(\frac{\pi\nu}{\delta}\left(\theta-\theta_j+\frac{\delta}{2}\right)\right)d\theta\tag{51}$$

$$\varepsilon_c(n,\nu,j)=\frac{2}{\delta}\int_{\theta_j-\delta/2}^{\theta_j+\delta/2}\cos(n\theta)\sin\left(\frac{\pi\nu}{\delta}\left(\theta-\theta_j+\frac{\delta}{2}\right)\right)d\theta.\tag{52}$$

The integral solutions are represented in Appendix B.

Overlapping windings- Based on the continuity condition between the two regions, the integration constants of the top part of the slots have been expressed in terms of the integration constants of the bottom part. Therefore in the case of 2-layer overlapping windings, (44) needs to be modified as

$$\begin{aligned}&n\left[a_n^a-b_n^a\left(\frac{R_r}{R_s}\right)^n\right]\\&-\sum_{j=1}^{N_s}\sum_{\nu=1}^{V}\frac{\pi\nu}{\delta}\left[\left(\frac{R_{slm}}{R_{sl}}\right)^{\frac{\pi\nu}{\delta}}\left(\frac{R_s}{R_{sl}}\right)^{\frac{\pi\nu}{\delta}}-\left(\frac{R_{slm}}{R_s}\right)^{\frac{\pi\nu}{\delta}}\right]\eta_c(n,\nu,j)b_\nu^{sl,j}\\&=\sum_{j=1}^{N_s}\frac{\mu_0}{2}\left[J_{b0}^j\left(R_{sl}^2-R_{slm}^2\right)+J_{t0}^j\left(R_{slm}^2-R_{so}^2\right)\right]\eta_c(n,0,j),\end{aligned}\tag{53}$$

(47) will be written as

$$\begin{aligned}&n\left[c_n^a-d_n^a\left(\frac{R_r}{R_s}\right)^n\right]\\&-\sum_{j=1}^{N_s}\sum_{\nu=1}^{V}\frac{\pi\nu}{\delta}\left[\left(\frac{R_{slm}}{R_{sl}}\right)^{\frac{\pi\nu}{\delta}}\left(\frac{R_s}{R_{sl}}\right)^{\frac{\pi\nu}{\delta}}-\left(\frac{R_{slm}}{R_s}\right)^{\frac{\pi\nu}{\delta}}\right]\eta_s(n,\nu,j)b_\nu^{sl,j}\\&=\sum_{j=1}^{N_s}\frac{\mu_0}{2}\left[J_{b0}^j\left(R_{sl}^2-R_{slm}^2\right)+J_{t0}^j\left(R_{slm}^2-R_{so}^2\right)\right]\eta_s(n,0,j)\end{aligned}\tag{54}$$

and (50) should be modified as

$$-\sum_{n=1}^{N} n\left\{\left[a_n^a + b_n^a\left(\frac{R_r}{R_s}\right)^n\right]\varepsilon_s(n,v,j) - \left[c_n^a + d_n^a\left(\frac{R_r}{R_s}\right)^n\right]\varepsilon_c(n,v,j)\right\} + \frac{\pi v}{\delta}\left[\left(\frac{R_{slm}}{R_{sl}}\right)^{\frac{\pi v}{\delta}}\left(\frac{R_s}{R_{sl}}\right)^{\frac{\pi v}{\delta}} + \left(\frac{R_{slm}}{R_s}\right)^{\frac{\pi v}{\delta}}\right] b_v^{sl,j} = 0. \tag{55}$$

Representing all the simultaneous equations in a matrix form yields

$$\begin{bmatrix} \mathbf{\Lambda}^{11} & \mathbf{\Lambda}^{12} & \mathbf{\Lambda}^{13} & \mathbf{\Lambda}^{14} & \mathbf{\Lambda}^{15} & \mathbf{0} \\ \mathbf{\Lambda}^{21} & \mathbf{\Lambda}^{22} & \mathbf{\Lambda}^{23} & \mathbf{0} & \mathbf{0} & \mathbf{0} \\ \mathbf{0} & \mathbf{\Lambda}^{32} & \mathbf{\Lambda}^{33} & \mathbf{0} & \mathbf{0} & \mathbf{\Lambda}^{36} \\ \mathbf{\Lambda}^{41} & \mathbf{0} & \mathbf{0} & \mathbf{\Lambda}^{44} & \mathbf{\Lambda}^{45} & \mathbf{0} \\ \mathbf{0} & \mathbf{0} & \mathbf{0} & \mathbf{\Lambda}^{54} & \mathbf{\Lambda}^{55} & \mathbf{\Lambda}^{56} \\ \mathbf{0} & \mathbf{\Lambda}^{62} & \mathbf{\Lambda}^{63} & \mathbf{\Lambda}^{64} & \mathbf{\Lambda}^{65} & \mathbf{\Lambda}^{66} \end{bmatrix} \begin{bmatrix} \mathbf{a}^{ra} \\ \mathbf{a}^{a} \\ \mathbf{b}^{a} \\ \mathbf{c}^{a} \\ \mathbf{d}^{a} \\ \mathbf{b}^{sl} \end{bmatrix} = \begin{bmatrix} \mathbf{0} \\ \mathbf{0} \\ \mathbf{\Gamma}^{3} \\ \mathbf{0} \\ \mathbf{\Gamma}^{5} \\ \mathbf{\Gamma}^{6} \end{bmatrix} \tag{56}$$

where

$$\mathbf{a}^{ra} = \left[a_1^{ra,1} \quad \dots \quad a_U^{ra,1} \quad \cdots \quad a_1^{ra,N_r} \quad \dots \quad a_U^{ra,N_r}\right]^{\mathrm{T}} \in \Re^{UN_r \times 1} \tag{57}$$

$$\mathbf{a}^{a} = \left[a_1^{a} \quad \cdots \quad a_N^{a}\right]^{\mathrm{T}} \in \Re^{N \times 1} \tag{58}$$

$$\mathbf{b}^{a} = \left[b_1^{a} \quad \cdots \quad b_N^{a}\right]^{\mathrm{T}} \in \Re^{N \times 1} \tag{59}$$

$$\mathbf{c}^{a} = \left[c_1^{a} \quad \cdots \quad c_N^{a}\right]^{\mathrm{T}} \in \Re^{N \times 1} \tag{60}$$

$$\mathbf{d}^{a} = \left[d_1^{a} \quad \cdots \quad d_N^{a}\right]^{\mathrm{T}} \in \Re^{N \times 1} \tag{61}$$

$$\mathbf{b}^{sl} = \left[b_1^{sl,1} \quad \dots \quad b_V^{sl,1} \quad \cdots \quad b_1^{sl,N_s} \quad \dots \quad b_V^{sl,N_s}\right]^{\mathrm{T}} \in \Re^{VN_s \times 1} \tag{62}$$

The sub-matrices $\mathbf{\Lambda}^{11} \in \Re^{UN_r \times UN_r}$, $\mathbf{\Lambda}^{22} \in \Re^{N \times N}$, $\mathbf{\Lambda}^{23} \in \Re^{N \times N}$, $\mathbf{\Lambda}^{32} \in \Re^{N \times N}$, $\mathbf{\Lambda}^{33} \in \Re^{N \times N}$, $\mathbf{\Lambda}^{44} \in \Re^{N \times N}$, $\mathbf{\Lambda}^{45} \in \Re^{N \times N}$, $\mathbf{\Lambda}^{54} \in \Re^{N \times N}$, and $\mathbf{\Lambda}^{55} \in \Re^{N \times N}$, are diagonal matrices in which sub-matrix $\mathbf{\Lambda}^{11}$ consists of N_r identical diagonal blocks and sub-matrix $\mathbf{\Lambda}^{66}$, consists of N_s identical diagonal blocks. In this study, to construct a diagonal or a block-diagonal matrix with identical blocks, one of its blocks is first expressed and the block is then replicated to form the matrix. The following convention is used in which the diagonal or block-diagonal matrix $\mathbf{\Lambda}^{xy}$ consists of a number of identical blocks $\hat{\mathbf{\Lambda}}^{xy}$:

$$\mathbf{\Lambda}^{xy} = \begin{bmatrix} \hat{\mathbf{\Lambda}}^{xy} & \mathbf{0} & \cdots & \mathbf{0} \\ \mathbf{0} & \hat{\mathbf{\Lambda}}^{xy} & & \mathbf{0} \\ \vdots & & \ddots & \\ \mathbf{0} & \mathbf{0} & & \hat{\mathbf{\Lambda}}^{xy} \end{bmatrix}. \tag{63}$$

The entries of the matrix-form simultaneous equations are represented in Appendix B. The integration constants are obtained by solving the simultaneous equations. Having calculated the integration constants, the radial and tangential components of the magnetic flux density in all regions can be predicted:

$$B_r^{ra,k}(r,\theta) = -\sum_{u=1}^{U} \frac{u\pi}{\beta} \frac{a_u^{ra,k}}{R_r}\left[\left(\frac{r}{R_r}\right)^{\frac{u\pi}{\beta}-1} + \left(\frac{R_{ra}}{R_r}\right)^{\frac{u\pi}{\beta}-1}\left(\frac{R_{ra}}{r}\right)^{\frac{u\pi}{\beta}+1}\right] \times \sin\left(\frac{u\pi}{\beta}\left(\theta - \alpha - \frac{2(k-0.5)\pi}{N_r} + \frac{\beta}{2}\right)\right) \tag{64}$$

$$B_\theta^{ra,k}(r,\theta) = -\sum_{u=1}^{U} \frac{u\pi}{\beta} \frac{a_u^{ra,k}}{R_r}\left[\left(\frac{r}{R_r}\right)^{\frac{u\pi}{\beta}-1} - \left(\frac{R_{ra}}{R_r}\right)^{\frac{u\pi}{\beta}-1}\left(\frac{R_{ra}}{r}\right)^{\frac{u\pi}{\beta}+1}\right] \times \cos\left(\frac{u\pi}{\beta}\left(\theta - \alpha - \frac{2(k-0.5)\pi}{N_r} + \frac{\beta}{2}\right)\right) \tag{65}$$

$$B_r^a(r,\theta)=-\sum_{n=1}^{N} n\left\{\left[\frac{a_n^a}{R_s}\left(\frac{r}{R_s}\right)^{n-1}+\frac{b_n^a}{R_r}\left(\frac{R_r}{r}\right)^{n+1}\right]\sin(n\theta)\right.$$
$$\left.-\left[\frac{c_n^a}{R_s}\left(\frac{r}{R_s}\right)^{n-1}+\frac{d_n^a}{R_r}\left(\frac{R_r}{r}\right)^{n+1}\right]\cos(n\theta)\right\} \tag{66}$$

$$B_\theta^a(r,\theta)=-\sum_{n=1}^{N} n\left\{\left[\frac{a_n^a}{R_s}\left(\frac{r}{R_s}\right)^{n-1}-\frac{b_n^a}{R_r}\left(\frac{R_r}{r}\right)^{n+1}\right]\cos(n\theta)\right.$$
$$\left.+\left[\frac{c_n^a}{R_s}\left(\frac{r}{R_s}\right)^{n-1}-\frac{d_n^a}{R_r}\left(\frac{R_r}{r}\right)^{n+1}\right]\sin(n\theta)\right\} \tag{67}$$

$$B_r^{sl,j}(r,\theta)=-\sum_{v=1}^{V}\frac{\pi v}{\delta}\left\{\frac{b_v^{sl,j}}{R_s}\right.$$
$$\times\left[\left(\frac{R_s}{R_{sl}}\right)^{\frac{\pi v}{\delta}+1}\left(\frac{r}{R_{sl}}\right)^{\frac{\pi v}{\delta}-1}+\left(\frac{R_s}{r}\right)^{\frac{\pi v}{\delta}+1}\right]$$
$$\left.+\frac{\mu_0 J_v^j}{\left(\frac{\pi v}{\delta}\right)^2-4}\left[r-\frac{2R_{sl}}{\frac{\pi v}{\delta}}\left(\frac{r}{R_{sl}}\right)^{\frac{\pi v}{\delta}-1}\right]\right\}$$
$$\times\sin\left(\tfrac{\pi v}{\delta}\left(\theta-\theta_j+\tfrac{\delta}{2}\right)\right) \tag{68}$$

$$B_\theta^{sl,j}(r,\theta)=\frac{-\mu_0 J_0^j}{2}\left(\frac{R_{sl}^2}{r}-r\right)$$
$$-\sum_{v=1}^{V}\left\{\frac{\pi v}{\delta}\frac{b_v^{sl,j}}{R_s}\left[\left(\frac{R_s}{R_{sl}}\right)^{\frac{\pi v}{\delta}+1}\left(\frac{r}{R_{sl}}\right)^{\frac{\pi v}{\delta}-1}-\left(\frac{R_s}{r}\right)^{\frac{\pi v}{\delta}+1}\right]\right.$$
$$\left.+\frac{2\mu_0 J_v^j}{\left(\frac{\pi v}{\delta}\right)^2-4}\left[r-R_{sl}\left(\frac{r}{R_{sl}}\right)^{\frac{\pi v}{\delta}-1}\right]\right\}\cos\left(\tfrac{\pi v}{\delta}\left(\theta-\theta_j+\tfrac{\delta}{2}\right)\right). \tag{69}$$

In the case of *overlapping windings* the radial and tangential components of the magnetic flux density in the top and bottom of the slots are expressed as

$$B_r^{slt,j}(r,\theta)=-\sum_{v=1}^{V}\frac{\pi v}{\delta}\frac{b_v^{sl,j}}{R_{slm}}\left[\left(\frac{R_{slm}}{R_{sl}}\right)^{\frac{\pi v}{\delta}+1}\left(\frac{r}{R_{sl}}\right)^{\frac{\pi v}{\delta}-1}\right.$$
$$\left.+\left(\frac{R_{slm}}{r}\right)^{\frac{\pi v}{\delta}+1}\right]\sin\left(\tfrac{\pi v}{\delta}\left(\theta-\theta_j+\tfrac{\delta}{2}\right)\right) \tag{70}$$

$$B_\theta^{slt,j}(r,\theta)=-\frac{\mu_0}{2}\left[J_{b0}^j\left(R_{sl}^2-R_{slm}^2\right)+J_{t0}^j\left(R_{slm}^2-r^2\right)\right]\frac{1}{r}$$
$$-\sum_{v=1}^{V}\frac{\pi v}{\delta}\frac{b_v^{sl,j}}{R_{slm}}\left[\left(\frac{R_{slm}}{R_{sl}}\right)^{\frac{\pi v}{\delta}+1}\left(\frac{r}{R_{sl}}\right)^{\frac{\pi v}{\delta}-1}\right.$$
$$\left.-\left(\frac{R_{slm}}{r}\right)^{\frac{\pi v}{\delta}+1}\right]\cos\left(\tfrac{\pi v}{\delta}\left(\theta-\theta_j+\tfrac{\delta}{2}\right)\right) \tag{71}$$

$$B_r^{slb,\,j}(r,\theta) = -\sum_{v=1}^{V} \frac{\pi v}{\delta} \frac{b_v^{sl,\,j}}{R_{slm}} \left[\left(\frac{R_{slm}}{R_{sl}} \right)^{\frac{\pi v}{\delta}+1} \left(\frac{r}{R_{sl}} \right)^{\frac{\pi v}{\delta}-1} + \left(\frac{R_{slm}}{r} \right)^{\frac{\pi v}{\delta}+1} \right] \times \sin\left(\frac{\pi v}{\delta} \left(\theta - \theta_j + \frac{\delta}{2} \right) \right) \tag{72}$$

$$B_\theta^{slb,\,j}(r,\theta) = \frac{-\mu_0 J_{b0}^{j}}{2} \left(R_{sl}^2 - r^2 \right) \frac{1}{r} - \sum_{v=1}^{V} \frac{\pi v}{\delta} \frac{b_v^{sl,\,j}}{R_{slm}} \left[\left(\frac{R_{slm}}{R_{sl}} \right)^{\frac{\pi v}{\delta}+1} \left(\frac{r}{R_{sl}} \right)^{\frac{\pi v}{\delta}-1} - \left(\frac{R_{slm}}{r} \right)^{\frac{\pi v}{\delta}+1} \right] \times \cos\left(\frac{\pi v}{\delta} \left(\theta - \theta_j + \frac{\delta}{2} \right) \right). \tag{73}$$

3. CASE STUDIES

To show the efficacy of the derived analytical magnetic field expressions, a three-phase slotted brushless DC (BLDC) motor with surface inset magnet and a switched reluctance motor are chosen. The brushless DC motor has 4 rotor-poles and 6 stator-slots and the switched reluctance motor is an 8/6 machine, i.e. 8-stator-pole and 6-rotor-pole. Table 1 lists the specifications of both motors.

Table 1. Specification of the studied machines

Parameter	Symbol		BLDC motor	SRM
Number of phases	q		3	4
Number of rotor poles	N_r		4	6
Number of stator poles	N_s		6	8
Stator outer radius	R_o	(mm)	48	50
Stator bottom slot radius	R_{sl}	(mm)	38	42
Stator bore radius	R_s	(mm)	26	28
Rotor outer radius	R_r	(mm)	25	27.5
Rotor bottom slot radius	R_{ra}	(mm)	18	18
Shaft radius	R_{sh}	(mm)	8	9
Stack length	L	(mm)	90	100
Stator slot span angle	δ	(rad/^{o})	0.440/25.2	0.419/24
Rotor slot span angle	β	(rad/^{o})	1.178/67.5	0.646/37
Rated phase current peak	I_m	(A)	10	10
Number of turn per pole	N_{turns}		102	123
Number of harmonics in all subdomains	N, U, V		200	200

a) Brushless DC motor

The armature reaction field distribution of the brushless DC (BLDC) motor is analytically calculated. The motor has a non-overlapping winding structure with all teeth wound. The three-phase armature currents are assumed to be in the form of the ideal rectangular waveforms shown in Appendix A.

The radial and tangential components of the armature reaction magnetic flux density at the middle of the air-gap are, respectively, depicted in Fig. 2(a)-(b) for the brushless DC motor having non-overlapping winding with all teeth wound at $\omega t = 0$ and $\omega t = \pi/4$ radians. Note that due to the symmetry only half of the 360^o-spatial position is illustrated.

The absolute value of the radial component of the flux density maximizes at those locations with minimum reluctance, i.e. when the rotor iron inter-poles are aligned with the stator teeth. As evident from Fig. 2(a), all four rotor iron inter-poles are partially aligned with slots at $\omega t = 0$. In contrast, only two of the rotor iron-inter-poles are fully aligned with the stator teeth at $\omega t = \pi/4$ radians. The analytical results

have been compared with those obtained from FEM and a good agreement between the analytical and numerical calculations has been observed.

The armature reaction flux density distribution of the brushless PM motor having non-overlapping winding with all teeth wound at $\omega t = 0$ and $\omega t = \pi/4$ radians is depicted in Figs. 3 and 4, respectively. In both cases the flux density reaches its maximum wherever the rotor iron inter-poles are aligned with the stator teeth. As evident from Fig. 3, phases B and C are carrying current at $\omega t = 0$. At $\omega t = \pi/4$ radians all three phases are active since a commutation between phases B and C is taking place, as shown in Fig. 4.

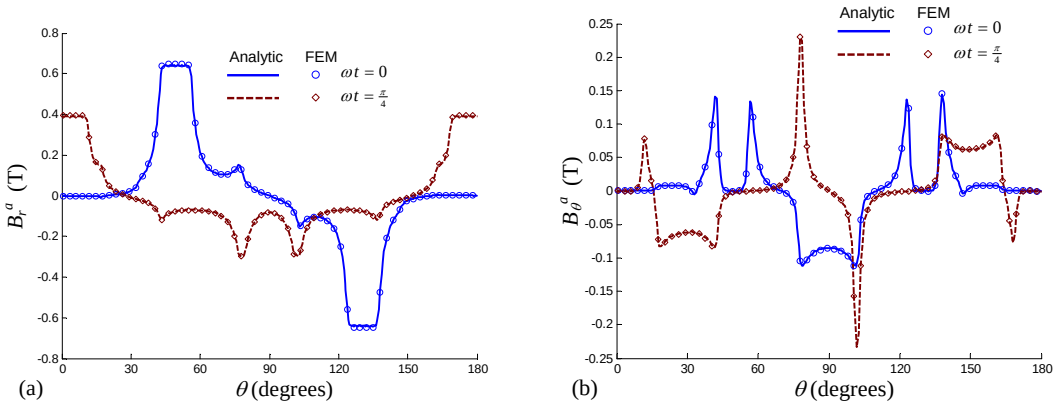

Fig. 2. (a) Radial and (b) tangential components of the armature reaction magnetic flux of the BLDC motor at $\omega t = 0$ and $\omega t = \pi/4$ radians where $\alpha_0 = \pi/4$ radians

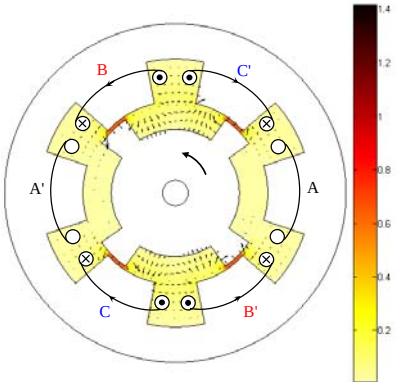

Fig. 3. Armature reaction magnetic flux density distribution at $\omega t = 0$ where $\alpha_0 = \pi/4$ radians in the case of the brushless PM machine with all teeth wound non-overlapping winding

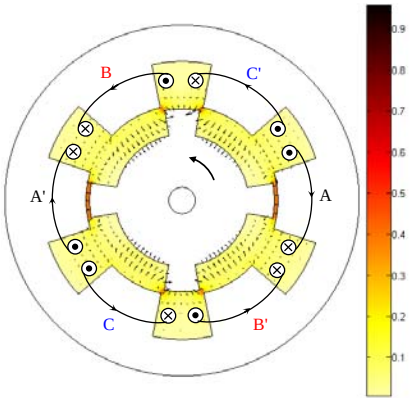

Fig. 4. Armature reaction magnetic flux density distribution at $\omega t = \pi/4$ radians where $\alpha_0 = \pi/4$ radians in the case of the brushless PM machine with all teeth wound non-overlapping winding. A commutation occurs between phases B and C

b) Switched reluctance motor

The magnetic flux distribution of a four-phase switched reluctance motor having 8 stator poles and 6 rotor poles is analytically calculated. Figure 5a-b respectively show the radial and tangential components of the magnetic flux density at two different rotor positions. The solid lines in Fig. 5 correspond to the instance in which current is commutated from phase D to phase A. The amplitude of the flux density seems to be well below the saturation point of back-iron B-H characteristic and therefore the proposed linear analytical solution is valid. However at $\omega t = \pi/24$ radians with $\alpha_0 = -\pi/12$ radians, as shown by dashed lines in Fig. 5, the magnetic flux density increases and the linear assumption can degrade the accuracy depending on the level of saturation. The magnetic flux distribution of the SRM at three rotor positions has been illustrated in Figs. 6-8.

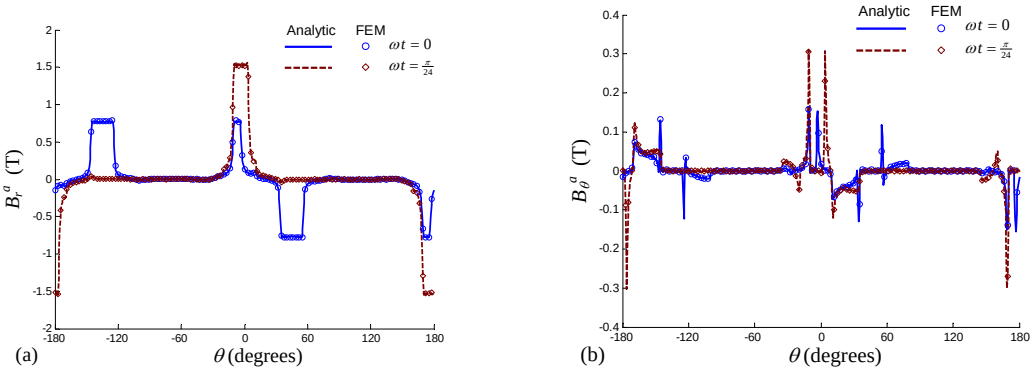

Fig. 5. (a) Radial and (b) tangential components of the magnetic flux of SRM at $\omega t = 0$ and $\omega t = \pi/24$ radians where $\alpha_0 = -\pi/12$ radians

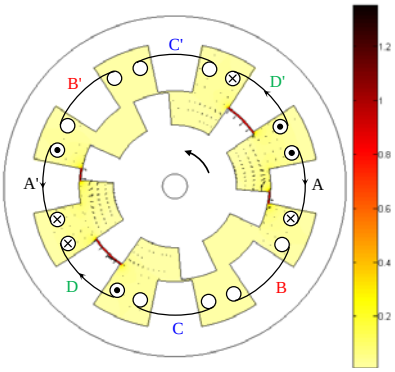

Fig. 6. Magnetic flux density distribution of the 8/6 SRM at $\omega t = 0$ where $\alpha_0 = -\pi/12$ radians without temporal overlapping current. Commutation between phases A and D

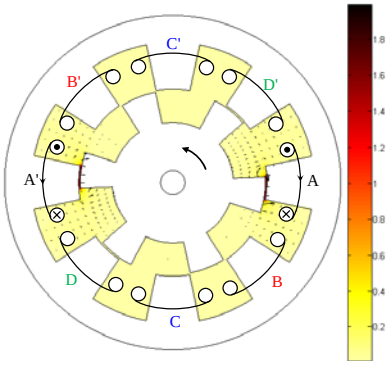

Fig. 7. Magnetic flux density distribution of the 8/6 SRM at $\omega t = \pi/24$ radians where $\alpha_0 = -\pi/12$ radians without temporal overlapping current

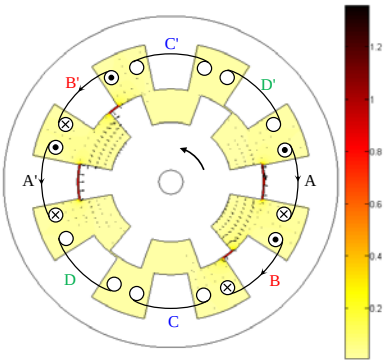

Fig. 8. Magnetic flux density distribution of the 8/6 SRM at $\omega t = \pi/12$ radians where $\alpha_0 = -\pi/12$ radians without temporal overlapping current. Commutation between phases A and B

4. CONCLUSION

Accurate magnetic field distribution of an electromagnetic device plays a vital role for its optimal design and critical analysis. A 2-D analytical magnetic field calculation has been proposed for doubly-salient machines. Comparing the analytical results with their corresponding numerical ones shows the accuracy and efficacy of the proposed approach for machines with negligible saturation effects. Even in those machines with considerable saturation effects at aligned rotor positions, the proposed analytical solution may be used at unaligned rotor positions in which the saturation effects are negligible. The proposed analytical magnetic field calculation method has been used in two case studies to illustrate the efficacy of the approach.

Acknowledgements: Portions of the work reported in this paper were funded by the Heptagon Fund, grant number QMUL-AD03; and portions were funded by the National Institute for Health Research (NIHR) Invention for Innovation (i4i) programme (II-FS-0110-14076). The views expressed in this publication are those of the authors and not necessarily those of the NHS, the NIHR or the Department of Health. The motors discussed as examples in this paper are much larger and of a different type than the motors designed for the products under development by the above grants.

REFERENCES

1. Boules, N. (1985). Prediction of no-load flux density distribution in permanent magnet machines. *IEEE Transactions on Industry Applications*, Vol. IA-21, No. 4, pp. 633-643.
2. Zhu, Z. Q., Howe, D., Bolte, E. & Ackermann, B. (1993). Instantaneous magnetic field distribution in brushless permanent magnet dc motors. Part I: Open-circuit field. *IEEE Transactions on Magnetics*, Vol. 29, No. 1, pp. 124-135.
3. Kim, U. & Lieu, D. K. (1998). Magnetic field calculation in permanent magnet motors with rotor eccentricity: Without slotting effect. *IEEE Transactions on Magnetics*, Vol. 34, No. 4, pp. 2243-2252.
4. Rasmussen, K. F., Davies, J. H., Miller, T.J.E., McGilp, M. I. & Olaru, M. (2000). Analytical and numerical computation of air-gap magnetic fields in brushless motors with surface permanent magnets. *IEEE Transactions on Industry Applications*, Vol. 36, No. 6, pp. 1547-1554.
5. Xia, Z. P., Zhu, Z. Q. & Howe, D. (2004). Analytical magnetic field analysis of halbach magnetized permanent-magnet machines. *IEEE Transactions on Magnetics*, Vol. 40, No. 4, pp. 1864-1872.
6. Markovic, M. & Perriard, Y. (2007). An analytical determination of eddy-current losses in a configuration with a rotating permanent magnet. *IEEE Transactions on Magnetics*, Vol. 43, No. 8, pp. 3380-3386.

7. Markovic, M. & Perriard, Y. (2009). Optimization design of a segmented halbach permanent-magnet motor using an analytical model. *IEEE Transactions on Magnetics*, Vol. 45, No. 7, pp. 2955-2960.
8. Rahideh, A. & Korakianitis, T. (2011). Analytical open-circuit magnetic field distribution of slotless brushless permanent magnet machines with rotor eccentricity. *IEEE Transactions on Magnetics*, Vol. 47, No. 12, pp. 4791-4808.
9. Kumar, P. & Bauer, P. (2008). Improved analytical model of a permanent-magnet brushless DC Motor. *IEEE Transactions on Magnetics*, Vol. 44, No. 10, pp. 2299-2309.
10. Zhu, Z. Q. & Howe, D. (1992). Analytical prediction of the cogging torque in radial-field permanent magnet brushless motors. *IEEE Transactions on Magnetics*, Vol. 28, No. 2, pp. 1371-1374.
11. [Zhu, Z. Q. & Howe, D. (1993). Instantaneous magnetic field distribution in brushless permanent magnet dc motors, Part III: Effect of stator slotting. *IEEE Transactions on Magnetics*, Vol. 29, No. 1, pp. 143-151.
12. Ackermann, B. & Sottek, R. (1995). Analytical modelling of the cogging torque in permanent magnet motors. *Electrical Engineering*, Vol. 78, pp. 117-125.
13. Kim, U. & Lieu, D. K. (1998). Magnetic field calculation in permanent magnet motors with rotor eccentricity: With slotting effect considered. *IEEE Transactions on Magnetics*, Vol. 34, No. 4, pp. 2253-2266.
14. Wang, X., Li, Q., Wang, S. & Li, Q. (2003). Analytical calculation of air-gap magnetic field distribution and instantaneous characteristics of brushless DC motors. *IEEE Transactions on Energy Conversion*, Vol. 18, No. 3, pp. 424-432.
15. Proca, A. B., Keyhani, A., EL-Antably, A., Lu, W. & Dai, M. (2003). Analytical model for permanent magnet motors with surface mounted magnets. *IEEE Transactions on Energy Conversion*, Vol. 18, No. 3, pp. 386-391.
16. Zarko, D., Ban, D. & Lipo, T. A. (2006). Analytical calculation of magnetic field distribution in the slotted air gap of a surface permanent-magnet motor using complex relative air-gap permeance. *IEEE Transactions on Magnetics*, Vol. 42, No. 7, pp. 1828-1837.
17. Liu, Z. J. & Li, J. T. (2007). Analytical solution of air-gap field in permanent-magnet motors taking into account the effect of pole transition over slots. *IEEE Transactions on Magnetics*, Vol. 43, No. 10, pp. 3872-3883.
18. Zarko, D., Ban, D. & Lipo, T. A. (2008). Analytical solution for cogging torque in surface permanent-magnet motors using conformal mapping. *IEEE Transactions on Magnetics*, Vol. 44, No. 1, pp. 52-65.
19. Liu, Z. J. & Li, J. T. (2008). Accurate prediction of magnetic field and magnetic forces in permanent magnet motors using an analytical solution. *IEEE Transactions on Energy Conversion*, Vol. 23, No. 3, pp. 717-726.
20. Liu, Z. J., Li, J. T. & Jiang, Q. (2008). An improved analytical solution for predicting magnetic forces in permanent magnet motors. *Journal of Applied Physics*, Vol. 103, No. 7, 07F135.
21. Boughrara, K., Chikouche, B. L., Ibtiouen, R., Zarko, D. & Touhami, O. (2009). Analytical model of slotted air-gap surface mounted permanent-magnet synchronous motor with magnet bars magnetized in the shifting direction. *IEEE Transactions on Magnetics*, Vol. 45, No. 2, pp. 747-758.
22. Dubas, F. & Espanet, C. (2009). Analytical solution of the magnetic field in permanent-magnet motors taking into account slotting effect: No-load vector potential and flux density calculation. *IEEE Transactions on Magnetics*, Vol. 45, No. 5, pp. 2097-2109.
23. Zhu, Z. Q., Wu, L. J. & Xia, Z. P. (2010). An accurate subdomain model for magnetic field computation in slotted surface mounted permanent magnet machines. *IEEE Transactions on Magnetics*, Vol. 46, No. 4, pp. 1100-1115.
24. Wu, L. J., Zhu, Z. Q., Staton, D., Popescu, M. & Hawkins, D. (2011). An improved subdomain model for predicting magnetic field of surface-mounted permanent-magnet machines accounting for tooth-tips. *IEEE Transactions on Magnetics*, Vol. 47, No. 6, pp. 1693-1704.
25. Zhu, Z. Q., Howe, D. & Chan, C. C. (2002). Improved analytical model for predicting the magnetic field distribution in brushless permanent-magnet machines. *IEEE Transactions on Magnetics*, Vol. 38, No. 1, pp. 229-238.

26. Holm, S. R., Polinder, H. & Ferreira, J. A. (2007). Analytical modeling of a permanent-magnet synchronous machine in a flywheel. *IEEE Transactions on Magnetics*, Vol. 43, No. 5, pp. 1955-1967.
27. Pfister, P. D. & Perriard, Y. (2011). Slotless permanent-magnet machines: general analytical magnetic field calculation. *IEEE Transactions on Magnetics*, Vol. 47, No. 6, pp. 1739-1752.
28. Boules, N. (1984). Two-dimensional field analysis of cylindrical machines with permanent magnet excitation. *IEEE Transactions on Industry Applications*, Vol. IA-20, No. 5, pp. 1267-1277.
29. Amara, Y., Reghem, P. & Barakat, G. (2010). Analytical prediction of eddy-current loss in armature windings of permanent magnet brushless AC machines. *IEEE Transactions on Magnetics*, Vol. 46, No. 8, pp. 3481-3484.
30. Lubin, T., Mezani, S. & Rezzoug, A. (2011). 2-D exact analytical model for surface-mounted permanent – magnet motors with semi-closed slots. *IEEE Transactions on Magnetics*, Vol. 47, No. 2, pp. 479-492.
31. Zhu, Z. Q. & Howe, D. (1993). Instantaneous magnetic field distribution in brushless permanent magnet dc motors, Part II: Armature-reaction field. *IEEE Transactions on Magnetics*, Vol. 29, No. 1, pp. 136-142.
32. Atallah, K., Zhu, Z. Q., Howe, D. & Birch, T. S. (1998). Armature reaction field and winding inductances of slotless permanent-magnet brushless machines. *IEEE Transactions on Magnetics*, Vol. 34, No. 5, pp. 3737-3744.
33. Zhu, Z. Q., Ng, K., Schofield, N. & Howe, D. (2004). Improved analytical modelling of rotor eddy current loss in brushless machines equipped with surface-mounted permanent magnets. *IEE Proc.-Electr. Power Appl.*, Vol. 151, No. 6, pp. 641-650.
34. Markovic, M. & Perriard, Y. (2008). Analytical solution for rotor eddy-current losses in a slotless permanent-magnet motor: The case of current sheet excitation. *IEEE Transactions on Magnetics*, Vol. 44, No. 3, pp. 386-393.
35. Ishak, D., Zhu, Z. Q. & Howe, D. (2005). Eddy-current loss in the rotor magnets of permanent-magnet brushless machines having a fractional number of slots per pole. *IEEE Transactions on Magnetics*, Vol. 41, No. 9, pp. 2462-2469.
36. Bellara, A., Amara, Y., Barakat, G. & Dakyo, B. (2009). Two-dimensional exact analytical solution of armature reaction field in slotted surface mounted PM radial flux synchronous machines. *IEEE Transactions on Magnetics*, Vol. 45, No. 10, pp. 4534-4538.
37. Wu, L. J., Zhu, Z. Q., Staton, D., Popescu, M. & Hawkins, D. (2011). Subdomain model for predicting armature reaction field of surface-mounted permanent-magnet machines accounting for tooth-tips. *IEEE Transactions on Magnetics*, Vol. 47, No. 4, pp. 812-822.
38. Rahideh, A. & Korakianitis, T. (2012). Subdomain analytical magnetic field prediction of slotted brushless machines with surface mounted magnets. *International Review of Electrical Engineering*, Vol. 7, No. 2.
39. Rahideh, A. & Korakianitis, T. (2012). Analytical magnetic field distribution of slotless brushless PM motors-Part I: Armature reaction field, inductance and rotor eddy current loss calculations. *IET Electric Power Applications*, Vol. 6, No. 9, pp. 628-638.
40. Rahideh, A. & Korakianitis, T. (2012). Analytical magnetic field distribution of slotless brushless PM motors-Part II: Open-circuit field and torque calculations. *IET Electric Power Applications*, Vol. 6, No. 9, pp. 639-651.
41. Rahideh, A. & Korakianitis, T. (2013). Analytical calculation of open-circuit field distribution of slotless brushless PM machines. *Electrical Power and Energy Systems*, Vol. 44, pp. 99-114.
42. Zhu, Z. Q., Howe, D. & Xia, Z. P. (1994). Prediction of open-circuit airgap field distribution in brushless machines having an inset permanent magnet rotor topology. *IEEE Transactions on Magnetics*, Vol. 30, No. 1, pp. 98-107.
43. Rahideh, A. & Korakianitis, T. (2011). Analytical magnetic field distribution of slotless brushless machines with inset permanent magnets. *IEEE Transactions on Magnetics*, Vol. 47, No. 6, pp. 1763-1774.

44. Rahideh, A., Mardaneh, M. & Korakianitis, T. (2013). Analytical 2D calculations of torque, inductance and back-EMF for brushless slotless machines with surface inset magnets. *IEEE Transactions on Magnetics*, In Press.
45. Jian, L., Chau, K. T., Gong, Y., Yu, C. & Li, W. (2009). Analytical calculation of magnetic field in surface-inset permanent-magnet motors. *IEEE Transactions on Magnetics*, Vol. 45, No. 10, pp. 4688-4691.
46. Boughrara, K., Zarko, D., Ibtiouen, R., Touhami, O. & Rezzoug, A. (2009). Magnetic field analysis of inset and surface-mounted permanent-magnet synchronous motors using Schwarz-Christoffel transformation. *IEEE Transactions on Magnetics*, Vol. 45, No. 8, pp. 3166-3178.
47. Rahideh, A. & Korakianitis, T. (2012). Analytical armature reaction field distribution of slotless brushless machines with inset permanent magnets. *IEEE Transactions on Magnetics*, Vol. 48, No. 7, pp. 2178-2191.
48. Rahideh, A. & Korakianitis, T. (2012). Analytical magnetic field calculation of slotted brushless PM machines with surface inset magnets. *IEEE Transactions on Magnetics*, Vol. 48, No. 10, pp. 2633-2649.
49. Lubin, T., Mezani, S. & Rezzoug, A. (2012). Two-dimensional analytical calculation of magnetic field and electromagnetic torque for surface-inset permanent magnet motors. *IEEE Transactions on Magnetics*, Vol. 48, No. 6, pp. 2080-2091.
50. Gysen, B. L. J., Meessen, K. J., Paulides, J. J. H. & Lomonova, E. A. (2010). General formulation of the electromagnetic field distribution in machines and devices using fourier analysis. *IEEE Transactions on Magnetics*, Vol. 46, No. 1, pp. 39-52.
51. Torrey, D. A. & Lang, J. H. (1990). Modelling a nonlinear variable-reluctance motor drive. *Proc. Inst. Electr. Eng*., vol. 137, no. 5, pp. 314-326.
52. Miller, T. J. E. & McGilp, M. (1990). Nonlinear theory of the switched reluctance motor for rapid computer-aided design. *Proc. Inst. Electr. Eng*., Vol. 137, No. 6, pp. 337-347.
53. Stephenson, J. M. & Corda, J. (1979). Computation of torque and current in doubly-salient reluctance motors from nonlinear magnetization data. *Proc. IEE*, Vol. 126, No. 5, pp. 393-396.
54. Xia, C. L., Xue, M. & Shi, T. N. (2009). A new nonlinear simulation method for switched reluctance motors. *IEEE Transactions on Energy Conversion*, Vol. 24, No. 3, pp. 578-586.
55. Lovatt, H. C. (2009). Analytical model of a classical switched-reluctance motor. *Proc. Inst. Electr. Eng*., Vol. 152, No. 2, pp. 352-358.
56. Lin, D., Zhou, P., Stanton, S. & Cendes, Z. J. (2009). An analytical circuit model of switched reluctance motors. *IEEE Transactions on Magnetics*, Vol. 45, No. 12, pp. 5368-5375.
57. Lubin, T., Mezani, S. & Rezzoug, A. (2010). Exact analytical method for magnetic field computation in the air-gap of cylindrical electric machines considering slotting effects. *IEEE Transactions on Magnetics*, Vol. 46, No. 4, pp. 1092-1099.
58. Rahman, K. M., Fahimi, B., Suresh, G., Rajarathnam, A. V. & Ehsani, M. (2000). Advantages of switched reluctance motor applications to EV and HEV: Design and control issues. *IEEE Transactions on Industry Applications*, Vol. 36, No. 1, pp. 111-121.
59. Miller, T. J. E. (2002). Optimal design of switched reluctance motors. *IEEE Transactions on Industrial Electronics*, Vol. 49, No. 1, pp. 15-27.
60. Dadpour, A. & Ansari, K. (2013). The effect of non-uniform air-gap on the noise in switched reluctance motors. *Iranian Journal of Science & Technology, Transactions of Electrical Engineering*, Vol. 37, No. E2, pp. 183-191.

APPENDIX A

Figures A1(a-c) show respectively the ideal phase currents of brushless DC (BLDC) motors, switched reluctance motors without temporal overlapping current and switched reluctance motors with temporal overlapping current.

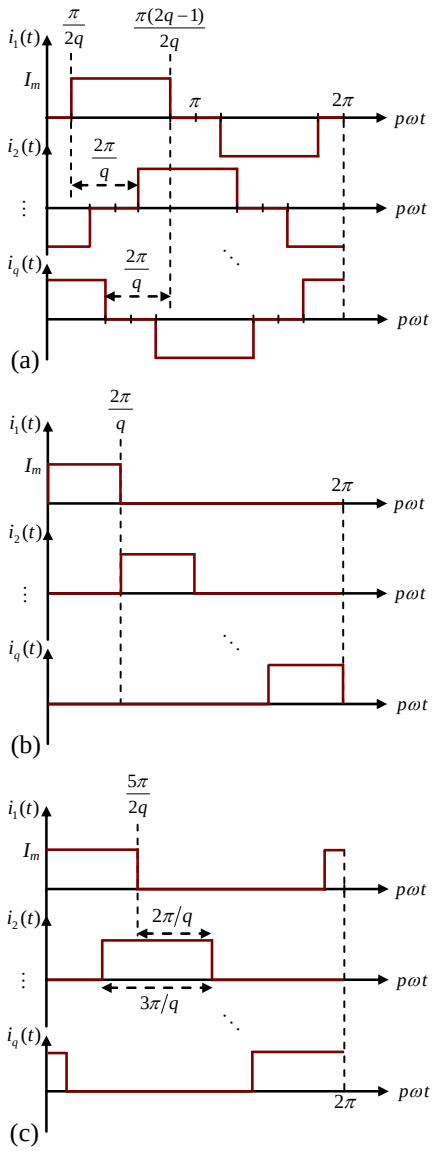

Fig. A1(a) Ideal current waveforms of a q-phase BLDC motor; (q-1) phases are conducting at each instant except at commutation times; (b) ideal current waveforms of a q-phase switched reluctance motor without temporal overlapping current; one phase is conducting at each instant except at commutation times; (c) ideal current waveforms of a q-phase switched reluctance motor with temporal overlapping current; one or two phases are conducting at each instant

The Fourier series expansion coefficients in the case of BLDC motors are expressed as

$$I_w = \frac{2I_m\left(1-(-1)^w\right)}{w\pi}\cos\left(\frac{w\pi}{2q}\right) \tag{A.1}$$

$$\theta_w = 0 \tag{A.2}$$

$$I_0 = 0 \tag{A.3}$$

where I_m is the maximum current. For switched reluctance motors without temporal overlapping current, these coefficients are expressed as follows:

$$I_w = \frac{2I_m}{w\pi}\left|\sin\left(\frac{w\pi}{q}\right)\right| \tag{A.4}$$

$$\theta_w = \tan^{-1}\left[\cot\left(\frac{w\pi}{q}\right)\right] \tag{A.5}$$

$$I_0 = \frac{I_m}{q}. \tag{A.6}$$

And finally in the case of switched reluctance motors with temporal overlapping current, the Fourier coefficients are expressed as

$$I_w = \frac{2I_m}{w\pi}\left|\sin\left(\frac{3w\pi}{2q}\right)\right| \tag{A.7}$$

$$\theta_w = \tan^{-1}\left[\frac{\sin\left(\frac{w\pi}{2q}\right)+\sin\left(\frac{5w\pi}{2q}\right)}{\cos\left(\frac{w\pi}{2q}\right)-\cos\left(\frac{5w\pi}{2q}\right)}\right] \tag{A.8}$$

$$I_0 = \frac{3I_m}{2q}. \tag{A.9}$$

APPENDIX B

The solutions of the integrals are

$$\sigma_s(n,u,k) = \frac{-\sin\left(u\pi+\frac{n\beta}{2}+n\alpha+\frac{2(k-0.5)n\pi}{N_r}\right)-\sin\left(\frac{n\beta}{2}-n\alpha-\frac{2(k-0.5)n\pi}{N_r}\right)}{n\beta+u\pi} - \frac{\sin\left(u\pi-\frac{n\beta}{2}-n\alpha-\frac{2(k-0.5)n\pi}{N_r}\right)-\sin\left(\frac{n\beta}{2}-n\alpha-\frac{2(k-0.5)n\pi}{N_r}\right)}{n\beta-u\pi} \tag{B.1}$$

$$\sigma_c(n,u,k) = \frac{-\cos\left(u\pi+\frac{n\beta}{2}+n\alpha+\frac{2(k-0.5)n\pi}{N_r}\right)+\cos\left(\frac{n\beta}{2}-n\alpha-\frac{2(k-0.5)n\pi}{N_r}\right)}{n\beta+u\pi} + \frac{\cos\left(u\pi-\frac{n\beta}{2}-n\alpha-\frac{2(k-0.5)n\pi}{N_r}\right)-\cos\left(\frac{n\beta}{2}-n\alpha-\frac{2(k-0.5)n\pi}{N_r}\right)}{n\beta-u\pi} \tag{B.2}$$

$$\rho_s(n,u,k) = \frac{-\beta}{2\pi} \times\left\{\frac{\cos\left(u\pi+\frac{n\beta}{2}+n\alpha+\frac{2(k-0.5)n\pi}{N_r}\right)-\cos\left(\frac{n\beta}{2}-n\alpha-\frac{2(k-0.5)n\pi}{N_r}\right)}{n\beta+u\pi} + \frac{\cos\left(u\pi-\frac{n\beta}{2}-n\alpha-\frac{2(k-0.5)n\pi}{N_r}\right)-\cos\left(\frac{n\beta}{2}-n\alpha-\frac{2(k-0.5)n\pi}{N_r}\right)}{n\beta-u\pi}\right\} \tag{B.3}$$

$$\rho_c(n,u,k) = \frac{\beta}{2\pi} \times\left\{\frac{\sin\left(u\pi+\frac{n\beta}{2}+n\alpha+\frac{2(k-0.5)n\pi}{N_r}\right)+\sin\left(\frac{n\beta}{2}-n\alpha-\frac{2(k-0.5)n\pi}{N_r}\right)}{n\beta+u\pi} - \frac{\sin\left(u\pi-\frac{n\beta}{2}-n\alpha-\frac{2(k-0.5)n\pi}{N_r}\right)-\sin\left(\frac{n\beta}{2}-n\alpha-\frac{2(k-0.5)n\pi}{N_r}\right)}{n\beta-u\pi}\right\} \tag{B.4}$$

for $n\beta \neq u\pi$ and

$$\sigma_s(n,u,k) = \frac{-1}{2n\beta}\left[\sin\left(3n\beta/2+n\alpha+\frac{2(k-0.5)n\pi}{N_r}\right) + \sin\left(n\beta/2-n\alpha-\frac{2(k-0.5)n\pi}{N_r}\right)\right] + \cos\left(n\beta/2-n\alpha-\frac{2(k-0.5)n\pi}{N_r}\right) \tag{B.5}$$

$$\sigma_c(n,u,k)=\frac{-1}{2n\beta}\Big[\cos\Big(3n\beta/2+n\alpha+\tfrac{2(k-0.5)n\pi}{N_r}\Big)-\cos\Big(n\beta/2-n\alpha-\tfrac{2(k-0.5)n\pi}{N_r}\Big)\Big]+\sin\Big(n\beta/2-n\alpha-\tfrac{2(k-0.5)n\pi}{N_r}\Big) \tag{B.6}$$

$$\rho_s(n,u,k)=\frac{-1}{4n\pi}\Big[\cos\Big(3n\beta/2+n\alpha+\tfrac{2(k-0.5)n\pi}{N_r}\Big)-\cos\Big(n\beta/2-n\alpha-\tfrac{2(k-0.5)n\pi}{N_r}\Big)\Big]-\frac{\beta}{2\pi}\sin\Big(n\beta/2-n\alpha-\tfrac{2(k-0.5)n\pi}{N_r}\Big) \tag{B.7}$$

$$\rho_c(n,u,k)=\frac{1}{4n\pi}\Big[\sin\Big(3n\beta/2+n\alpha+\tfrac{2(k-0.5)n\pi}{N_r}\Big)+\sin\Big(n\beta/2-n\alpha-\tfrac{2(k-0.5)n\pi}{N_r}\Big)\Big]+\frac{\beta}{2\pi}\cos\Big(n\beta/2-n\alpha-\tfrac{2(k-0.5)n\pi}{N_r}\Big) \tag{B.8}$$

for $n\beta=u\pi$.

$$\eta_s(n,v,j)=\frac{\delta^2 n}{\pi}\frac{(-1)^v\cos\big(n(\theta_j+\frac{\delta}{2})\big)-\cos\big(n(\theta_j-\frac{\delta}{2})\big)}{\pi^2v^2-\delta^2n^2} \tag{B.9}$$

$$\eta_c(n,v,j)=\frac{\delta^2 n}{\pi}\frac{(-1)^{v+1}\sin\big(n(\theta_j+\frac{\delta}{2})\big)+\sin\big(n(\theta_j-\frac{\delta}{2})\big)}{\pi^2v^2-\delta^2n^2} \tag{B.10}$$

$$\varepsilon_s(n,v,j)=2\pi v\frac{(-1)^{v+1}\sin\big(n(\theta_j+\frac{\delta}{2})\big)+\sin\big(n(\theta_j-\frac{\delta}{2})\big)}{\pi^2v^2-\delta^2n^2} \tag{B.11}$$

$$\varepsilon_c(n,v,j)=2\pi v\frac{(-1)^{v+1}\cos\big(n(\theta_j+\frac{\delta}{2})\big)+\cos\big(n(\theta_j-\frac{\delta}{2})\big)}{\pi^2v^2-\delta^2n^2} \tag{B.12}$$

for $\pi v\neq\delta n$ and

$$\eta_s(n,v,j)=\frac{\sin\big(n(\theta_j-\frac{\delta}{2})\big)}{2\pi/\delta}-\frac{\cos\big(n(\theta_j+\frac{3\delta}{2})\big)-\cos\big(n(\theta_j-\frac{\delta}{2})\big)}{4n\pi} \tag{B.13}$$

$$\eta_c(n,v,j)=\frac{\cos\big(n(\theta_j-\frac{\delta}{2})\big)}{2\pi/\delta}+\frac{\sin\big(n(\theta_j+\frac{3\delta}{2})\big)-\sin\big(n(\theta_j-\frac{\delta}{2})\big)}{4n\pi} \tag{B.14}$$

$$\varepsilon_s(n,v,j)=\cos\big(n(\theta_j-\tfrac{\delta}{2})\big)-\frac{\sin\big(n(\theta_j+\frac{3\delta}{2})\big)-\sin\big(n(\theta_j-\frac{\delta}{2})\big)}{2n\delta} \tag{B.15}$$

$$\varepsilon_c(n,v,j)=-\sin\big(n(\theta_j-\tfrac{\delta}{2})\big)-\frac{\cos\big(n(\theta_j+\frac{3\delta}{2})\big)-\cos\big(n(\theta_j-\frac{\delta}{2})\big)}{2n\delta} \tag{B.16}$$

for $\pi v=\delta n$.

From Eq. (34) the entries of the sub-matrices on the first row of the matrix-form simultaneous Eq., (56), can be found,

$$\hat{\Lambda}^{11}_{u,u}=\frac{u\pi}{\beta}\left[1+\left(\frac{R_{ra}}{R_r}\right)^{\frac{2u\pi}{\beta}}\right] \tag{B.17}$$

$$\Lambda^{12}_{u+(k-1)U,n}=-n\left(\frac{R_r}{R_s}\right)^n\sigma_s(n,u,k) \tag{B.18}$$

$$\Lambda^{13}_{u+(k-1)U,n}=-n\sigma_s(n,u,k) \tag{B.19}$$

$$\Lambda^{14}_{u+(k-1)U,n}=n\left(\frac{R_r}{R_s}\right)^n\sigma_c(n,u,k) \tag{B.20}$$

$$\Lambda^{15}_{u+(k-1)U,n}=n\sigma_c(n,u,k) \tag{B.21}$$

From Eq. (41) the entries of the sub-matrices on the second row of the matrix-form simultaneous Eq. (56), can be found,

$$\Lambda^{21}_{n,u+(k-1)U} = \frac{u\pi}{\beta}\left[\left(\frac{R_{ra}}{R_r}\right)^{\frac{2u\pi}{\beta}} - 1\right]\rho_c(n,u,k) \tag{B.22}$$

$$\Lambda^{22}_{n,n} = n\left(\frac{R_r}{R_s}\right)^n \tag{B.23}$$

$$\Lambda^{23}_{n,n} = -n \tag{B.24}$$

From Eq. (44) the entries of the sub-matrices on the third row of the matrix-form simultaneous Eq. (56), in the case of *non-overlapping windings* can be found,

$$\Lambda^{32}_{n,n} = n \tag{B.25}$$

$$\Lambda^{33}_{n,n} = -n\left(\frac{R_r}{R_s}\right)^n \tag{B.26}$$

$$\Lambda^{36}_{n,v+(j-1)V} = -\frac{\pi v}{\delta}\left[\left(\frac{R_s}{R_{sl}}\right)^{\frac{2\pi v}{\delta}} - 1\right]\eta_c(n,v,j) \tag{B.27}$$

$$\begin{aligned}\Gamma^3_{n,1} &= \sum_{j=1}^{N_s}\frac{\mu_0 J_0^j}{2}\left(R_{sl}^2 - R_s^2\right)\eta_c(n,0,j) \\ &+ \sum_{j=1}^{N_s}\sum_{v=1}^{V}\frac{2\mu_0 J_v^j}{\left(\frac{\pi v}{\delta}\right)^2 - 4}\left[R_s^2 - R_{sl}^2\left(\frac{R_s}{R_{sl}}\right)^{\frac{\pi v}{\delta}}\right]\eta_c(n,v,j)\end{aligned} \tag{B.28}$$

and in the case of *overlapping windings* the last two Eq. (B.27) and (B.28), are modified as follows using (53):

$$\begin{aligned}\Lambda^{36}_{n,v+(j-1)V} = -\frac{\pi v}{\delta}&\left[\left(\frac{R_{slm}}{R_{sl}}\right)^{\frac{\pi v}{\delta}}\left(\frac{R_s}{R_{sl}}\right)^{\frac{\pi v}{\delta}} - \left(\frac{R_{slm}}{R_s}\right)^{\frac{\pi v}{\delta}}\right] \\ &\times\eta_c(n,v,j)\end{aligned} \tag{B.29}$$

$$\Gamma^3_{n,1} = \sum_{j=1}^{N_s}\frac{\mu_0}{2}\left[J_{b0}^j\left(R_{sl}^2 - R_{slm}^2\right) + J_{t0}^j\left(R_{slm}^2 - R_s^2\right)\right]\eta_c(n,0,j) \tag{B.30}$$

From Eq. (38) the entries of the sub-matrices on the fourth row of the matrix-form simultaneous Eq. (56), can be found,

$$\Lambda^{41}_{n,u+(k-1)U} = \frac{u\pi}{\beta}\left[\left(\frac{R_{ra}}{R_r}\right)^{\frac{2u\pi}{\beta}} - 1\right]\rho_s(n,u,k) \tag{B.31}$$

$$\Lambda^{44}_{n,n} = n\left(\frac{R_r}{R_s}\right)^n \tag{B.32}$$

$$\Lambda^{45}_{n,n} = -n \tag{B.33}$$

From Eq. (47) the entries of the sub-matrices on the fifth row of the matrix-form simultaneous Eq. (56), in the case of *non-overlapping windings* can be found,

$$\Lambda^{54}_{n,n} = n \tag{B.34}$$

$$\Lambda_{n,n}^{55} = -n\left(\frac{R_r}{R_s}\right)^n \tag{B.35}$$

$$\Lambda_{n,\,v+(j-1)V}^{56} = -\frac{\pi v}{\delta}\left[\left(\frac{R_s}{R_{sl}}\right)^{\frac{2\pi v}{\delta}} - 1\right]\eta_s(n,v,j) \tag{B.36}$$

$$\begin{aligned}\Gamma_{n,1}^{5} = &\sum_{j=1}^{N_s}\frac{\mu_0 J_0^j}{2}\left(R_{sl}^2 - R_s^2\right)\eta_s(n,0,j)\\ &+\sum_{j=1}^{N_s}\sum_{v=1}^{V}\frac{2\mu_0 J_v^j}{\left(\frac{\pi v}{\delta}\right)^2-4}\left[R_s^2 - R_{sl}^2\left(\frac{R_s}{R_{sl}}\right)^{\frac{\pi v}{\delta}}\right]\eta_s(n,v,j)\end{aligned} \tag{B.37}$$

and in the case of *overlapping windings* based on (54) the last two Eq. (B.36) and (B.37), are modified as

$$\begin{aligned}\Lambda_{n,\,v+(j-1)V}^{56} = -\frac{\pi v}{\delta}&\left[\left(\frac{R_{slm}}{R_{sl}}\right)^{\frac{\pi v}{\delta}}\left(\frac{R_s}{R_{sl}}\right)^{\frac{\pi v}{\delta}} - \left(\frac{R_{slm}}{R_s}\right)^{\frac{\pi v}{\delta}}\right]\\ &\times\eta_s(n,v,j)\end{aligned} \tag{B.38}$$

$$\Gamma_{n,1}^{5} = \sum_{j=1}^{N_s}\frac{\mu_0}{2}\left[J_{b0}^j\left(R_{sl}^2 - R_{slm}^2\right) + J_{t0}^j\left(R_{slm}^2 - R_s^2\right)\right]\eta_s(n,0,j) \tag{B.39}$$

From Eq. (50) the entries of the sub-matrices on the sixth row of the matrix-form simultaneous Eq. (56), in the case of *non-overlapping windings* can be found,

$$\Lambda_{v+(j-1)V,n}^{62} = -n\varepsilon_s(n,v,j) \tag{B.40}$$

$$\Lambda_{v+(j-1)V,n}^{63} = -n\left(\frac{R_r}{R_s}\right)^n\varepsilon_s(n,v,j) \tag{B.41}$$

$$\Lambda_{v+(j-1)V,n}^{64} = n\varepsilon_c(n,v,j) \tag{B.42}$$

$$\Lambda_{v+(j-1)V,n}^{65} = n\left(\frac{R_r}{R_s}\right)^n\varepsilon_c(n,v,j) \tag{B.43}$$

$$\hat{\Lambda}_{v,v}^{66} = \frac{\pi v}{\delta}\left[\left(\frac{R_s}{R_{sl}}\right)^{\frac{2\pi v}{\delta}} + 1\right] \tag{B.44}$$

$$\Gamma_{v+(j-1)V,1}^{6} = -\frac{\mu_0 J_v^j}{\left(\frac{\pi v}{\delta}\right)^2-4}\left[\frac{\pi v}{\delta}R_s^2 - 2R_{sl}^2\left(\frac{R_s}{R_{sl}}\right)^{\frac{\pi v}{\delta}}\right] \tag{B.45}$$

and in the case of *overlapping windings* based on (55) the last two Eq. (B.44) and (B.45), are modified as

$$\hat{\Lambda}_{v,v}^{66} = \frac{\pi v}{\delta}\left[\left(\frac{R_{slm}}{R_{sl}}\right)^{\frac{\pi v}{\delta}}\left(\frac{R_s}{R_{sl}}\right)^{\frac{\pi v}{\delta}} + \left(\frac{R_{slm}}{R_s}\right)^{\frac{\pi v}{\delta}}\right] \tag{B.46}$$

$$\Gamma_{v+(j-1)V,1}^{6} = 0 \tag{B.47}$$